Far-field superfocusing with an optical fiber based surface plasmonic lens made of nanoscale concentric annular slits

Yuxiang Liu,[1] Hua Xu,[2, 3] Felix Stief,[1] Nikolai Zhitenev,[2] and Miao Yu[1, 3, *]

[1]*Department of Mechanical Engineering, University of Maryland, College Park, MD 20742, USA*
[2]*Center for Nanoscale Science and Technology, National Institute of Standards and Technology, Gaithersburg, MD 20899 USA*
[3]*Maryland NanoCenter, University of Maryland, College Park, MD 20742*
[*]*mmyu@umd.edu*

Abstract: We present experimental demonstration of light superfocusing by using an optical fiber based surface plasmonic (SP) lens with nanoscale concentric annular slits. A far-field, sub-diffraction-limit sized focus was achieved with an optical fiber based device. The performance of SP lenses with three and four annular slits was experimentally characterized. Guidelines and suggestions on designing the SP lens are provided. As a microscale device with nanoscale features, the fiber-based SP lens can provide a solution to bridging nanophotonics and conventional optics.

OCIS codes: (240.6680) Surface plasmons; (310.6628) Subwvelength structures, nanostructures; (060.2310) Fiber optics.

References and links

1. L. Verslegers, P. B. Catrysse, Z. Yu, and S. Fan, "Planar metallic nanoscale slit lenses for angle compensation" Appl. Phys. Lett. **95**, 071112 (2009).
2. F. Duerr, Y. Meuret, and H. Thienpont, "Miniaturization of Frensnel lenses for solar concentration: a quantitative investigation," Appl. Optics **49**, 2339-2346 (2010).
3. M. Born and E. Wolf, *Principles of Optics, 7th (expanded) ed.* (Cambridge University Press, Cambridge, 2003).
4. V. P. Kalosha and I. Golub, "Toward the subdiffraction focusing limit of optical superresolution," Opt. Lett. **32**, 3540-3542 (2007).
5. W. L. Barnes, A. Dereux, and T. W. Ebbesen, "Surface plasmon subwavelength optics," Nature **424**, 824-830 (2003).
6. Z. Liu, J. M. Steele, W. Srituravanich, Y. Pikus, C. Sun, and X. Zhang, "Focusing surface plasmons with plasmonic lens," Nano Lett. **5**, 1726-1729 (2005).
7. W. Chen, D. C. Abeysinghe, R. L. Nelson, and Q. Zhan, "Plasmonic lens made of multiple concentric metallic rings under radially polarized illumination," Nano Lett. **9**, 4320-4325 (2009).
8. Y. Fu, Y. Liu, X. Zhou, Z. Xu, and F. Fang, "Experimental investigation of superfocusing of plasmonic lens with chirped circular nanoslits," Opt. Express **18**, 3438-3443 (2010), http://www.opticsinfobase.org/oe/abstract.cfm?uri=oe-18-4-3438.
9. L. Verslegers, P. B. Catrysse, Z. Yu, J. S. White, E. S. Barnard, M. L. Brongersma, and S. Fan, "Planar lenses based on nanoscale slit arrays in a metallic film," Nano Lett. **9**, 235-238 (2009).
10. L. Lin, X. M. Goh, L. P. McGuinness, and A. Roberts, "Plasmonic lenses formed by two-dimensional nanometric cross-shaped aperture arrays for Fresnel-region focusing" Nano Lett. **10**, 1936-1940 (2010).
11. E. J. Smith, Z. Liu, Y. Mei, and O. G. Schmidt, "Combined surface plasmon and classical waveguiding through metamaterial fiber design," Nano Lett. **10**, 1-5 (2010).
12. A. R. Zakharian, J. V. Moloney, and M. Mansuripur, "Surface plasmon polaritons on metallic surfaces," Opt. Express **15**, 183-197 (2007), http://www.opticsinfobase.org/oe/abstract.cfm?uri=oe-15-1-183.
13. Z. Bomzon, V. Kleiner, E. Hasman, "Formation of radially and azimuthally polarized light using space-variant subwavelength metal stripe gratings," Appl. Phys. Lett. **79**, 1587 (2001).
14. A. G. Curto, A. Manjavacas, and F. J. Garcia de Abajo, "Near-field focusing with optical phase antennas," Opt. Express **17**, 17801-17811 (2009), http://www.opticsinfobase.org/oe/abstract.cfm?uri=oe-17-20-17801.

15. H. Shi, C. Wang, C. Du, X. Luo, X. Dong, and H. Gao, "Beam manipulating by metallic nano-slits with variant widths," Opt. Express **13**, 6815-6820 (2005), http://www.opticsinfobase.org/abstract.cfm?URI=oe-13-18-6815
16. E. D. Palik, *Handbook of optical constants of solid* (Academic Press, San Diego, 1998).
17. P. B. Catrysse and S. Fan, "Understanding the dispersion of coaxial plasmonic structures through a connection with the planar metal-insulator-metal geometry," Appl. Phys. Lett. **94**, 231111 (2009).
18. L. Cai, J. Zhang, W. Bai, Q. Wang, X. Wei, and G. Song, "Generation of compact radially polarized beam at 850 nm in vertical-cavity surface-emitting laser via plasmonic modulation," Appl. Phys. Lett. **97**, 201101 (2010).
19. H. Ko, H. C. Kim, and M. Cheng, "Light focusing at metallic annular slit structure coated with dielectric layers," Appl. Opt. **49**, 950-954 (2010).
20. Y. Yu and H. Zappe, "Effect of lens size on the focusing performance of plasmonic lenses and suggestions for the design," Opt. Express **19**, 9434-9444 (2011), http://www.opticsinfobase.org/abstract.cfm?URI=oe-19-10-9434.
21. P. Ruffieux, T. Scharf, H. Herzig, R. Völkel, and K. Weible, "On the chromatic aberration of microlenses," Opt. Express **14**, 4687-4694 (2006), http://www.opticsinfobase.org/oe/abstract.cfm?uri=oe-14-11-4687.
22. S. Nesson, M. Yu, X. M. Zhang, and A. Hsieh, "Miniature fiber optic pressure sensor with composite polymer-metal diaphragm for intradiscal pressure measurements," J. Biomed. Opt. **13**, 0044040 (2008).
23. H. Bae, X. Zhang, H. Liu, and M. Yu, "Miniature surface-mountable Fabry-Perot pressure sensor constructed with a 45° angled fiber," Opt. Lett. **35**, 1701-1703 (2010).
24. Y. Fu, W. Zhou, L. E. N. Lim, C. L. Du, and X. G. Luo, "Plasmonic microzone plate: superfocusing at visible regime," Appl. Phys. Lett. **91**, 061124 (2007).
25. F. Garcia-Vidal, L. Martin-Moreno, T. Ebbesen, and L. Kuipers, "Light passing through subwavelength apertures," Rev. Mod. Phys. **82**, 729-787 (2010).
26. H. Schouten, T. Visser, and D. Lenstra, "Light transmission through a subwavelength slit: waveguiding and optical vortices," Phys. Rev. E **67**, 036608 (2003).
27. Z. Bomzon, V. Kleiner, and E. Hasman, "Formation of radially and azimuthally polarized light using space-variant subwavelength metal stripe gratings," Appl. Phys. Lett. **79**, 1587-1589 (2001).
28. F. Wang, M. Xiao, K. Sun, and Q. Wei, "Generation of radially and azimuthally polarized light by optical transmission through concentric circular nanoslits in Ag films," Opt. Express **18**, 63-71 (2010), http://www.opticsinfobase.org/oe/abstract.cfm?uri=oe-18-1-63.

1. Introduction

Miniaturization of photonic devices has become increasingly important. Specifically, high performance miniature lenses are essential for the development of solid-state image sensors [1] and solar cells [2]. However, when the conventional optics is used, the focal size is inevitably limited by the Abbe's diffraction limit ($0.51\lambda/NA$), which is defined as the full width at half-maximum (FWHM) of the Airy disk [3, 4]. Here, λ is the wavelength in vacuum and *NA* is the numerical aperture of the lens. Moreover, the performance of conventional spherical lenses deteriorates as their sizes approach the wavelength. When the focal length becomes comparable or even larger than the lens aperture size, it becomes even more difficult to achieve a high numerical aperture as well as a sub-diffraction-limit focal size. Recent progress in surface plasmon polaritons (SPPs) has provided promising solutions to achieving compact photonic devices through manipulation of SPPs [5]. While focusing of SPPs has been readily achieved in the near field [6-8], far-field focusing of propagating light in the medium is more desirable, which can help prevent possible physical contact or interference between the focusing devices and the samples. Recently, far-field focusing has been experimentally demonstrated by using SP lenses fabricated on glass substrates with nanoscale patterns such as one-dimensional slit arrays [9] and cross-shaped aperture arrays [10]. Compared with glass substrates, optical fibers have been serving as classical low-loss waveguides for decades. In order to combine SPPs and classical waveguiding, metamaterial based optical fiber designs have been proposed in a recent study [11].

In this paper, to combine the classical fiber optic technology and the emerging field of SPPs, we present an SP lens directly fabricated on the endface of a classical single-mode optical fiber for achieving far-field superfocusing in both transverse dimensions. This work provides a solution to overcoming the diffraction limit as well as bridging the nanophotonics

and conventional optics with an optical fiber based SP device. The fiber-based SP lens can be readily integrated into many existing systems for a variety of applications including laser nanofabrication, optical trapping, high-density optical storage, and high-resolution fluorescence sensing.

2. Working principle and design

The fiber-based SP lens is composed of a set of concentric annular slits with varied nanoscale widths, which are formed on a uniform gold coating that covers the endface of a single-mode optical fiber, as shown in Fig. 1(a). When the linearly polarized light guided in the fiber impinges on the SP lens, SPPs are excited at the slit edges [6]. Since the transverse electric (TE) propagating modes cannot exist in SPPs [12], only the radially polarized light components can pass through the slits in the form of transverse magnetic (TM) modes of SPPs, if the slit is small enough compared with the wavelength. These TM mode SPPs will be coupled back to optical waves at the exit of the slit, rendering in-phase radial polarization [13] of the exiting light waves.

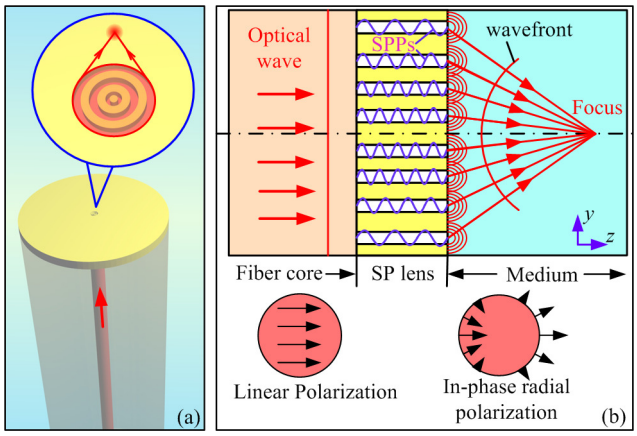

Fig. 1. (a) Schematic of a surface plasmonic lens formed on the endface of an optical fiber. (b) Schematic of the design model of the fiber-based SP lens. The two circles with arrows show the polarization states of the light in fiber core (linear polarized) and in the medium (in-phase radially polarized).

The starting design of SP lens is based on geometric optics for achieving a far-field focus in water, as shown in Fig. 1(b). In order to achieve constructive interference at a tentative focal length f_0 (here, f_0 is chosen to be 20 μm), the total phase delays induced by different slits should differ by integer times 2π, i.e.,

$$2\pi n_d \frac{\sqrt{r_i^2 + f_0^2} - \sqrt{r_{i+1}^2 + f_0^2}}{\lambda} + \mathrm{Re}(\beta_i - \beta_{i+1})d = 2\pi N, \qquad (1)$$

where r_i is the i-th slit radius, β_i is the propagation constant of the SPPs in the i-th slit, d is the thickness of the gold layer, n_d is the refractive index of water (n_d =1.33), λ is the free space wavelength, and N is an integer. The propagation constant of the SPPs, β_i, is dependent on the slit width. The first term of Eq. (1) describes the phase delay difference of the propagating waves exiting from the adjacent slits, while the second term stands for that of the SPPs in the adjacent slits. A similar lens design with nanoscale concentric rings was reported [14], with the focusing effect resulting from light scattering at the rings instead of propagation of SPPs.

The dispersion relation of the TM modes can be approximately expressed as [9, 15]

$$\tanh\left[\frac{w_i}{2}\sqrt{\beta_i^2 - k_0^2\varepsilon_d}\right] = -\frac{\varepsilon_d\sqrt{\beta_i^2 - k_0^2\varepsilon_m}}{\varepsilon_m\sqrt{\beta_i^2 - k_0^2\varepsilon_d}}, \quad (2)$$

where w_i is the width of the i-th slit, k_0 the propagation constant of light in vacuum, ε_d the permittivity of the dielectrics in the slit (1.77 for water), and ε_m the permittivity of the metal (-27.0+1.9i for gold at $\lambda = 808$ nm [16]). It is noted that more rigorous models are needed to provide a more precise analysis of SPPs propagation for ring diameters less than the optical wavelength [17]. However, Eq. (1) can still provide a reasonable approximation for the SPPs propagation in ring-shaped structures [18, 19].

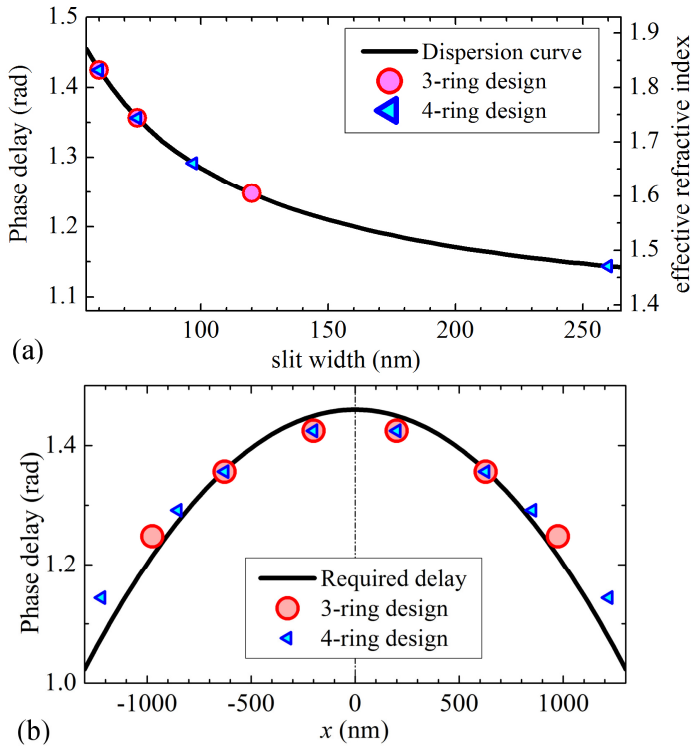

Fig. 2. (a) Dependence of the phase delay and effective index on the width of a water slit in gold. (b) Dependence of the phase delay on the slit radius to achieve a focus in water. The gold layer thickness is 100 nm. The two inner annular slits of the 3-ring design and 4-ring design share the same widths and radii.

The phase delay and refractive index required to achieve a focus at f_0 are obtained according to Eq. (2), which are shown as the solid curve in Fig. 2(a). For a smaller slit width, the optical part of the SPPs will be confined tighter to the surface, and thus more of the modes will penetrate into the metal, resulting in a higher real part of the effective refractive index (β_i/k_0) and a larger phase delay. The targeted phase delay calculated from Eq. (1) as a function of radial positions is shown as the solid curve in Fig. 2(b). Two designs with different numbers of annular slits (referred to as 3-ring and 4-ring designs) are also included in Fig. 2. Following these designs, the planar SP lens will induce a curved wavefront, which can help focus the optical waves. It is noted that the phase delays induced by the designed devices slightly deviate from the required values, as shown in Fig. 2(b). This will ensure that the separations between the adjacent slits are sufficient to prevent the sidewalls from collapsing during the fabrication process. To have enough light intensity incident on the SP lens, the

radius of the outermost slit is designed to be smaller than the beam waist of the fundamental guided mode in the optical fiber (~2.8 μm). The annular slits can result in a tighter focus compared to a circular aperture with the same diameter [3] due to the smaller diffraction limit. In this regard, the subwavelength annular slit design of the fiber-based SP lens can work as a diffractive focusing lens as well as a radial polarizer to help filter out the non-radially polarized components in the incident light.

However, the performance of the SP lens can depend on effects that are not considered in the design principles discussed above. Most importantly, the focal length can be affected by the size of the SP lens, resulting in a large discrepancy between the design and the experiment [9, 20]. The effects of the lens size have been theoretically investigated in a recent work [20]. For a small SP lens, the focus shifts towards the lens due to the strong diffraction effects at the aperture stop. Only when the lens size is large enough so that the diffraction effects are weak, the obtained focal length can be close to the designed value. To estimate the real focal length of a small lens, a method developed for conventional microlenses [21] can be used. The method was demonstrated to provide good results particularly for small SP lenses with a total phase difference (the phase difference at the lens exit between the outermost ring and the lens axis) less than 0.6π [20]. The strength of the diffraction can be characterized by the Fresnel number (*FN*), which can be written as

$$FN = \frac{\rho^2 n_d}{\lambda f_0} \ , \tag{3}$$

where ρ is the lens size (the outer ring radius of the SP lens). For an incident plane wave with an intensity of I_0, the on-axis intensity distribution after the lens can be approximated by the Rayleigh-Sommerfeld integral as

$$I(z) = 4I_0 \sin\left(\frac{\pi\rho^2}{2\lambda z}\right)^2 \ . \tag{4}$$

The location of the maximum intensity, z_m, can be found as

$$z_m = \frac{\rho^2}{\lambda} \ . \tag{5}$$

When *FN* is less than 1, the focal length approaches z_m due to the strong diffraction effects. In our case, both the 3-ring and 4-ring designs have an *FN* much less than 1 and a total phase difference less than 0.6π, so z_m can provide a good estimation for the focal length according to the model used in [20]. Based on Eq. (5), z_m is calculated to be 1.7 μm and 3.0 μm for the 3-ring and 4-ring SP lenses, respectively.

3. Fabrication and experimental setup

The fabrication started with deposition of 100-nm-thick gold (Au 99.999%, ACI Alloys) layer with a 3-nm-thick titanium adhesion layer on the cleaved endface of 808 nm single-mode fibers (SM800, Fibercore) by using E-beam evaporation (BJD-1800, Temescal). The slits were then fabricated by using Focus Ion Beam (FIB) milling (NVision 40, Carl Zeiss SMT AG).

To study the performance of the SP lens, the fiber was mounted vertically on a microscope with the SP lens facing an oil-immersion objective lens (Olympus PlanC 100×/1.25). The fiber end together with the SP lens was submerged in a water drop on a coverglass. A motorized stage with a resolution of 20 nm was used to move the fiber along the vertical direction. Light from a pigtailed 808 nm laser diode was coupled into the fiber. The intensity distribution of the output beam at the focal plane of the objective lens was recorded by a digital camera with a 12-bit dynamic range sampling the focal plane at 60 nm (nominal value, see Section 5 for more detail) per pixel. The boundary of each pixel served as a pinhole in the image plane yielding better resolution of the intensity distribution as described in reference [9]. Three-dimensional (3D) intensity maps were reconstructed from the captured images taken with a step of 100 nm in the vertical direction. Compared with the near-field

measurement techniques, such as the NSOM technique, this method of intensity measurements does not distort the field distribution.

4. Experimental results

The experimentally measured intensity profiles of the 3-ring SP lens are shown in Fig. 3. A tight focus in three dimensions is clearly seen with the maximum intensity obtained at z=1.2±0.5 μm. The *NA* of this SP lens was calculated to be 0.91 in water according to the focal length of 1.2 μm. The focal plane intensity profile along the x axis is shown in Fig. 3(g). The transverse spot sizes defined by the FWHM were found to be 340±60 nm ($0.38\lambda/NA$) along the x direction and 420±60 nm ($0.47\lambda/NA$) along the y direction. Similar focusing effects were observed from another SP lens with 4 annular slits, as shown Fig. 4. The focus of the 4-ring SP lens was obtained at around z=3.1±0.5 μm, which is longer than that obtained from the 3-ring device, and its *NA* was calculated to be 0.56 in water. As can be seen in Fig. 4(c) and (h), the focus obtained from the 4-ring SP lens has much better quality with smaller side lobes compared with that obtained from the 3-ring device. The transverse spot sizes of the 4-ring device were measured to be 450±60 nm ($0.31\lambda/NA$) along the x direction and 500±60 nm ($0.34\lambda/NA$) along the y direction. Note that the transverse focal sizes obtained from both fiber-based SP lenses were smaller than the diffraction limit ($0.51\lambda/NA$). Based on the intensity profiles along the z axis, as shown in Fig. 5, the depths of focus (FWHM) were obtained as 0.74±0.10 μm ($1.2\lambda/n_d$) and 1.76±0.10μm ($2.9\lambda/n_d$) for the 3-ring and 4-ring SP lenses, respectively. The transmission of the optical power is measured to be 5.5% and 15.4% for the 3-ring and 4-ring SP lenses, respectively.

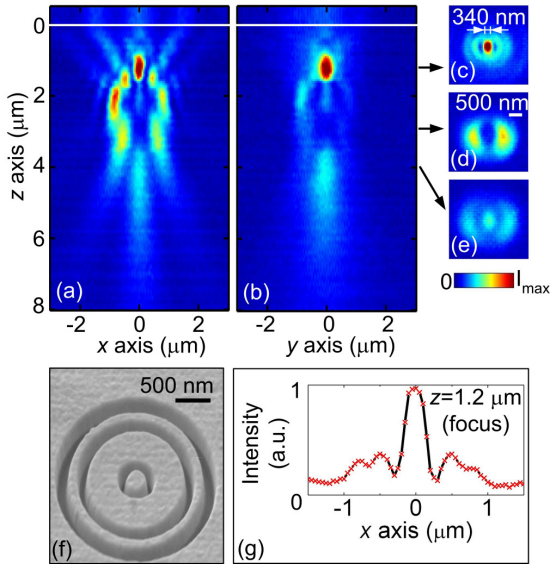

Fig. 3. Intensity profiles obtained with the 3-ring SP lens in the (a) xz and (b) yz planes. The fiber faced downwards with the endface (the white line) located at z=0 and the z axis being the optical axis. (c)-(e) Intensity profiles in the xy planes at z = 1.2 μm, 3 μm, and 4 μm, respectively. (f) SEM image of the 3-ring SP lens. (g) The intensity along the x axis at z=1.2 μm (focus).

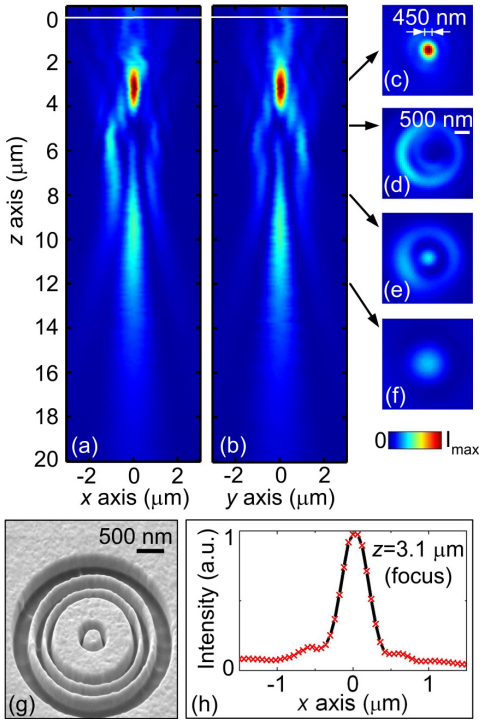

Fig. 4. Intensity profiles obtained with the 4-ring SP lens in the (a) xz and (b) yz planes. The fiber faced downwards with the endface (the white line) located at z=0 and the z axis being the optical axis. (c)-(f) Intensity profiles in the xy planes at z = 3.1 μm, 5 μm, 8 μm, and 12 μm, respectively. (g) SEM image of the 4-ring SP lens. (h) The intensity along the x axis at z=3.1 μm (focus).

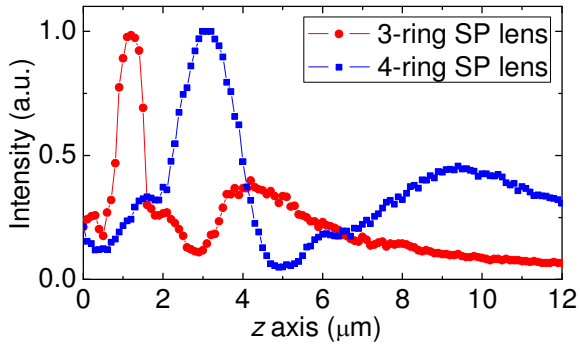

Fig. 5. The intensity distributions along the optical axis obtained from the two SP lenses.

5. Validity of the intensity measurement method using a CCD camera

To verify that our intensity measurement method can indeed resolve the details of the intensity fields of the SP lenses, we demonstrated that the SP lens movement of less than 100 nm can be resolved from the CCD images. A high-resolution fiber optic Fabry-Perot interferometer (FPI) was used to measure the actual movement of the SP lens, and the measurements served as the reference for comparison with those obtained from the imaging displacements measured by the CCD camera. The experimental setup for calibrating the camera measurement is shown in Fig. 6. The FPI setup and principles have been described in our previous work [22, 23]. The Fabry-Perot cavity was formed between a fixed mirror and

the end of an optic fiber that was fixed to a motorized stage (Zyvex S200, Zyvex Instruments, LLC). The motorized stage can provide movements with a resolution of 2 nm based on the manufacturer data. The fiber based SP lens was fixed to the same stage next to the fiber of the FPI system. As the stage was moved, the stage displacement can be obtained by the cross correlation of the camera images and by the output spectrum of the FPI. The displacement measurements using the two methods were then compared. The FPI measurements have a displacement resolution of 3.5 nm [23], which is sufficient to provide a faithful calibration for the imaging method.

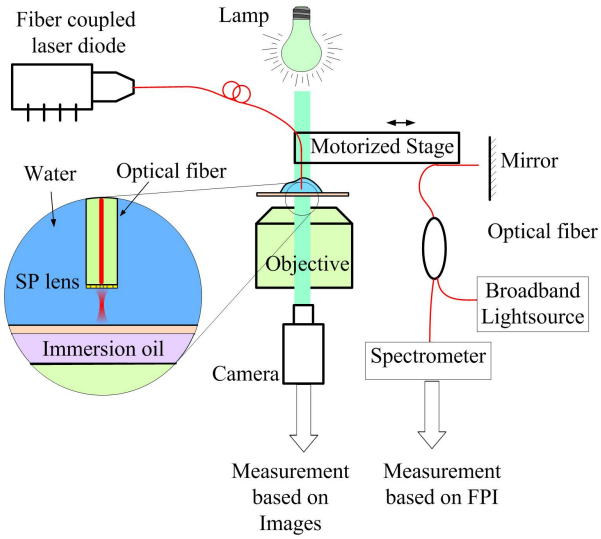

Fig. 6. Experimental arrangement for validation of the camera imaging method.

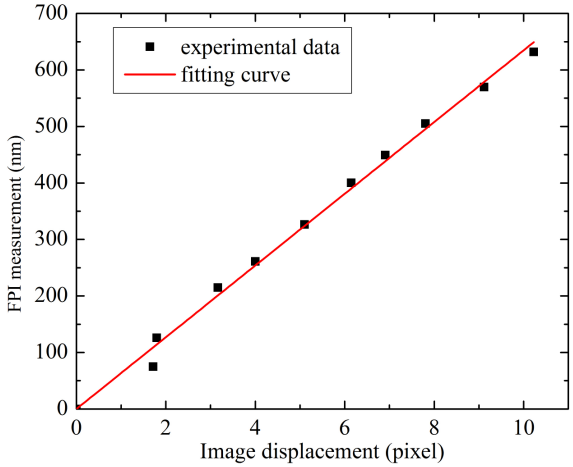

Fig. 7. A typical calibration curve of the camera imaging method. The *x* axis is the image displacement obtained with the camera imaging method, while the *y* axis is that obtained with the Fabry-Perot interferometer (FPI) method. The slope of linear fit is 63.5 nm/pixel.

A typical set of measurement results is shown in Fig. 7. The slope of the linear fit is the approximate resolution of the displacement measurement of the imaging method. According

to seven measurements (other six data sets not shown), the camera imaging method has an average resolution of 61.1±3.6 nm/pixel, and a mechanical displacement (the separation between two adjacent data points) of ~60 nm is readily detectable. The fact that the detectable displacement is below 100 nm proves that the camera imaging method does oversample the optical field of the SP lens, similar to the confocal scanning optical microscope used in reference [9]. Therefore, the measurement results provided in Section 4 are faithful.

6. Discussion

6.1 x- and y-axis differences and overestimation of focal sizes

According to the results shown in Fig. 3 and Fig. 4, the transverse focal sizes along the x and y directions are slightly different. This difference can be caused by the linear polarization of the incident light. Such difference in transverse focal sizes has also been observed in a previous theoretical study on a SP lens comprising annular slits in metal [24].

It should be pointed out that the real transverse spot sizes are expected to be even smaller than the measured values. First, due to the point spread function (Airy disk), the image at the image plane of the objective, which is detected by the camera, will be inevitably blurred. Second, the intensity obtained at each pixel of the camera was the averaged value over the entire pixel area, which can cause an underestimation of the highest intensity. Both issues can result in an overestimation of the spot sizes. These overestimation effects are expected to be more serious for smaller focal sizes (e.g., the focus of the 3-ring SP lens).

6.2 Comparison of focal lengths and focal depths of two SP lenses

The comparison between the experimental results of the 3-ring and 4-ring SP lenses (see Fig. 5) indicates that, with a larger number of annular slits, a longer depth of focus can be realized. A long depth of focus can be useful in nanolithography for fabrication of structures with a high aspect ratio. On the other hand, the focal lengths obtained in the experiments (1.2 μm for the 3-ring lens and 3.1 μm for the 4-ring lens) agree well with the ones predicted by z_m (1.7 μm for the 3-ring lens and 3.0 μm for the 4-ring lens) in Eq. (5) of the diffraction model. Note that z_m values are significantly smaller than the focal length designed by Eq. (1) of the geometric optics (f_0 =20 μm). This confirms that the small lens sizes in our design can result in strong diffraction effects and thus, the focuses shift towards the lenses. Similar aperture effects have also been reported in a previous experimental study on one dimensional SP lenses [9]. The minor discrepancy between the measured focal lengths and those predicted by Eq. (5) can be caused by the measurement error of the position of the fiber surface. In the experiment, the fiber surface was assigned to the position of the sharpest image of the ring patterns.

6.3 Different symmetry of the intensity profiles of the 3-ring and 4-ring fibers

In addition to the difference in the focal lengths, the intensity patterns of the two SP lenses also display different kinds of symmetry. The transverse intensity distributions obtained from the 3-ring SP lens exhibit obvious mirror symmetry (see Fig. 3(a)-(e)), while those obtained from the 4-ring SP lens are closer to rotational symmetry (see Fig. 4(a)-(f)). The difference in the transverse focal sizes is also larger for the 3-ring SP lens. The difference in the symmetry can be explained by a higher transmission of the azimuthal polarization components for the 4-ring SP lens. In our design model, we assume that the slit widths are small enough so that the SPPs can only propagate in the slits in the form of TM modes (in-phase radially polarized components). However, if the free-space wavelength of the incident s-polarized light is smaller than a cutoff value λ_c, conventional TE modes can also be coupled into the slits. For a slit sidewall made of perfect electric conductors (PECs), the cutoff wavelength λ_c is $2w/n_{diel}$ [25]. Here w is the slit width and n_{diel} the index of refraction of the dielectric medium in the slit. We have designed the slit widths to ensure that at the working wavelength of 808 nm, the conventional TE modes will become evanescent and suffer from significant attenuation [25]. However, the cutoff wavelength in a real metal is larger than that in the PEC due to the

limited conductivity [26], which can result in partial transmission of the conventional TE modes [25], especially for slits with large widths. Note that the outermost slits are 120 nm and 260 nm in width for the 3-ring and 4-ring SP lenses, respectively. Therefore, we expect that there will be considerable amount of conventional TE modes in the outermost slit of the 4-ring SP lens, which can be coupled into in-phase azimuthally polarized optical waves [27] at the exit of the SP lens. The evidence of such azimuthally polarized components obtained with annular slits has been reported previously when small wavelengths or large slit widths are used [28]. Note that both the TM and TE modes exhibit mirror symmetry of the intensity, but about different axes. Since there is a combination of the radial and azimuthal polarization, the intensity fields of the 4-ring SP lens become more rotationally symmetric, rendering less difference in the *xz* and *yz* plane intensity distributions. In the case of the 3-ring SP lens, due to the small slit widths that only allow for transmission of TM mode SPPs, the transverse intensity distributions exhibit mirror symmetry as expected. It is noted that the slight asymmetry in Fig. 4(a) and (b) is believed to be a consequence of the misalignment between the SP lens and the fiber core during the fabrication.

6.4 Misalignment between the rings and the fiber core

During the fabrication process, the misalignment between the rings and fiber core was carefully accessed. According to the SEM images (data not shown), the fabrication misalignment of the rings with respect to the fiber core was found to be less than 1 μm, with a typical misalignment of ~0.5 μm along both *x* and *y* directions. For a misalignment much smaller than the mode field diameter of the optical fiber, the design principles (Eqs. (1) and (2)) still hold for achieving the constructive interference because of the flat wavefront of the optical wave guided in a single-mode fiber. The misalignment (say, along the *x* axis) can introduce an asymmetry (with respect to the *y* axis) to the illumination of the SP lens and hence a distortion to the intensity of the focus. However, since the light intensity in the fiber core follows Gaussian distribution with a mode field diameter of 5.6 μm, a misalignment of less than 1 μm will not significantly affect the performance of the focus. In the experiment, we did not observe any noticeable distortion to the intensity distributions at the focuses (see Fig. 3 and Fig. 4), which confirms that the effects of the misalignment are not significant.

6.5 Guidelines and suggestions for designing fiber-based SP lens

For fiber based SP lenses, the lens sizes are limited by the small core size of the single-mode fiber. Therefore, the diffraction effects have to be considered when the lenses are designed. For example, the focal length is mainly influenced by the diffraction and can be estimated by Eq. (5). For a larger number of slits, the lens size increases, and hence a longer focal length as well as a longer focal depth can be obtained. However, in order to ensure the desired spherical wave front, the outer slit widths have to be larger, resulting in smaller separations between the slits. Due to the limitation of the fabrication process, for a 100-nm-thick gold layer, we can only realize a 4-ring device. If the slit widths can be better controlled in the fabrication process, one more annular slit could be added between the two innermost slits, rendering a 5-ring device that can potentially have a longer focal length and better performance. The optimum thickness of the metal layer for the SP lens performance is affected by certain trade-offs. For a fixed slit width, a thicker metal layer can introduce a larger phase delay, and thus it seems that more slits can be included in the design. However, a thicker metal poses fabrication challenges. In applications that require a uniform and rotationally symmetric transverse intensity distribution at the focus, a circular polarization maintaining optical fiber can be useful. In addition, since the SP lens is located within the fiber core area, if preferred, the fiber can be thinned to further increase the compactness of the device without deteriorating the focusing performance.

7. Conclusions

Far-field superfocusing in both transverse directions has been achieved with a fiber-based SP lens. A focal spot with a transverse focal size as small as $0.31\lambda/NA$ (450 nm) at a wavelength of 808 nm that is below diffraction limit has been experimentally demonstrated The long depth of focus with a small transverse focal size enables high resolution fabrication of high aspect ratio structures in nanolithography. By combining the conventional fiber optic technology and the emerging nanophotonics, the fiber-based SP lens offers a solution to bridging nanophotonic devices and macroscale optical components. The fiber-based SP lens may find applications in high-resolution imaging, nanoparticle acceleration and manipulation, subwavelength direct laser writing, and biological sensing.

Acknowledgements

Support received from NSF (CMMI1031331) is gratefully acknowledged. This work was also partially supported by the NIST-CNST/UMD-Nanocenter Cooperative Agreement. The authors would like to thank the staff of the NanoFab at the Center for Nanoscale Science and Technology for the help with the fabrication process development. The authors also acknowledge the support of the Maryland NanoCenter and its FabLab and NispLab. The NispLab is supported in part by the NSF as a MRSEC Shared Experimental Facility.